Results in Engineering 23 (2024) 102573

Contents lists available at ScienceDirect

Results in Engineering

journal homepage: www.sciencedirect.com/journal/results-in-engineering

Semiconductors for enhanced solar photovoltaic-thermoelectric 4E performance optimization: Multi-objective genetic algorithm and machine learning approach

Hisham Alghamdi [a], Chika Maduabuchi [b,*], Aminu Yusuf [c,d,**], Sameer Al-Dahidi [e,***], Sedat Ballikaya [c], Abdullah Albaker [f], Ahmed Alsafran [g], Mohammed Alghassab [h], Emad Makki [i], Mohammad Alkhedher [j]

[a] Electrical Engineering Department, College of Engineering, Najran University, Najran, 55461, Saudi Arabia
[b] Artificial Intelligence Laboratory, University of Nigeria Nsukka, Nsukka, 410001, Enugu State, Nigeria
[c] Department of Engineering Sciences, Istanbul University – Cerrahpaşa, Avcılar, Istanbul, 34320, Turkey
[d] Department of Electrical and Electronics Engineering, Federal University-Dutsinma, Katsina, P.M.B 5001, Nigeria
[e] Department of Mechanical and Maintenance Engineering, School of Applied Technical Sciences, German Jordanian University, Amman, 11180, Jordan
[f] Department of Electrical Engineering, College of Engineering, University of Ha'il, Ha'il, 81451, Saudi Arabia
[g] Department of Electrical Engineering, College of Engineering, King Faisal University, Alahsa, 31982, Saudi Arabia
[h] Electrical Engineering Department, College of Engineering, Shaqra University, Riyadh, 11911, Saudi Arabia
[i] Department of Mechanical Engineering, College of Engineering and Islamic Architecture, Umm Al-Qura University, Makkah, 24382, Saudi Arabia
[j] Department of Mechanical and Industrial Engineering, Abu Dhabi University, Abu Dhabi, 59911, United Arab Emirates

ARTICLE INFO

Keywords:
Photovoltaics
Thermoelectric module
Genetic algorithm
Artificial neural networks

ABSTRACT

In this study, a groundbreaking exploration of a concentrated photovoltaic-thermoelectric (CPV-TE) module employing an unprecedented selection of six thermoelectric materials across diverse temperature ranges is presented. This work innovatively employs a multi-objective optimization framework that combines genetic algorithms and goal attainment methods, aiming to optimize energy, exergy, environmental, and economic (4 E) performance. Notably, this study is the first to construct and evaluate five regression-based machine learning models with an emphasis on minimal root mean squared error and mean absolute error for rapid CPV-TE performance predictions, essential for real-world applications. Our analysis unveils that among the tested materials, the CPV-TE module incorporating lead telluride (PbTe) achieves the highest 4 E performance, demonstrating a peak exergy efficiency of 14.2 %, and annual energy savings and carbon reduction of 13.5 kWh and 6.4 kg, respectively. Furthermore, the Gaussian Process Regression model is identified as the most effective among the machine learning models for forecasting performance across the materials. This study significantly advances the field by providing novel insights into thermoelectric material selection and optimization for CPV-TE modules, and establishing pioneering forecasting tools that catalyze the efficient deployment of these systems.

Symbol/ Abbreviation	Description	Units
A	Area of PV/TEG	m^2
A_{pv}	Surface area of the PV	m^2
A_{te}	Surface area of the TEG	m^2
$BiTe$	Bismuth Telluride	–
C	Concentration ratio	–

(continued on next column)

(*continued*)

cde_{ele}	Coefficient of CO2 saving	kg/kWh
C_i	Initial investment	$
CO_2	Carbon dioxide	–
$CoSb$	Cobalt Antimonide	–
CPV	Concentrated Photovoltaic	–
CRF	Capital Recovery Factor	–

(continued on next page)

* Corresponding author.
** Corresponding author. Department of Engineering Sciences, Istanbul University – Cerrahpaşa, Avcılar, Istanbul, 34320, Turkey.
*** Corresponding author.
E-mail addresses: chika.maduabuchi.191341@unn.edu.ng (C. Maduabuchi), aminu.yusuf@iuc.edu.tr (A. Yusuf), sameer.aldahidi@gju.edu.jo (S. Al-Dahidi).

https://doi.org/10.1016/j.rineng.2024.102573
Received 14 May 2024; Received in revised form 6 July 2024; Accepted 14 July 2024
Available online 16 July 2024

(*continued*)

E_c	First-year energy cost	$\$(kWh)^{-1}$
ERT	Ensembles of Regression Trees	–
E_{sys}	Annual energy	kWh
G	Solar irradiance	W/m^2
GPR	Gaussian Process Regression	–
G_s	Solar irradiance at standard test conditions	W/m^2
h	Heat transfer coefficient	$W/(m^2{\cdot}K)$
HMS	Higher Manganese Silicide	–
I	Electric current of a single thermocouple	mA
i_f	Inflation rate	%
IRR	Internal Rate of Return	–
k_n	Thermal conductivity of n-type TE leg	$W/(m{\cdot}K)$
k_p	Thermal conductivity of p-type TE leg	$W/(m{\cdot}K)$
L	Length of the TE leg	mm
$LCOE$	Levelized Cost of Energy	–
$LiNiO$	Lithium Nickel Oxide	–
MAE	Mean Absolute Error	–
ML	Machine Learning	–
N	Number of thermocouples	–
NN	Neural Networks	–
NPV	Net Present Value	–
PBP	Payback Period	years
$PbTe$	Lead Telluride	–
PCA	Principal Component Analysis	–
P_{pv}	Output power generated by the PV	W
P_{te}	Output power generated by the TEG	W
PV	Photovoltaic	–
Q_c	Heat released from the cold side of the TEG	W
Q_h	Heat absorbed by the hot side of the TEG	W
R	Internal resistance of a single thermocouple	Ω
R_{con}	Contact resistance	Ω
R_{kt}	Thermal resistance of the TEG	K/W
$RMSE$	Root Mean Square Error	–
RT	Regression Trees	–
S_c	Seebeck coefficient of the cold side of the TEG	μV/K
S_h	Seebeck coefficient of the hot side of the TEG	μV/K
SVM	Support Vector Machines	–
T	Absolute temperature	K
T_a	Ambient temperature	°C
T_c	Temperature of the cold side of the TEG	K
TE	Thermoelectric	–
TEG	Thermoelectric Generator	–
T_h	Temperature of the hot side of the TEG	K
T_{pv}	Temperature of the PV	K
T_s	Solar temperature	K
v	Wind speed measured at a height of 10 m	m/s
β	Temperature coefficient of the PV	K^-1
ΔT	Temperature difference between the PV surface and back sheet	°C
η_r	Reference efficiency of the PV	%
η_{sys}	Energy efficiency of the CPV-TE system	%
σ_n	Electrical conductivity of n-type TE leg	S/m
σ_p	Electrical conductivity of p-type TE leg	S/m
τ	Thomson coefficient	μV/K
τ_g	Transmissivity of the glass	–
Ψ_{sys}	Exergy efficiency of the CPV-TE system	%

1. Introduction

Fossil fuels and nuclear power account for over 66 % and 8 % of global energy production, respectively, according to the Central Intelligence Agency [1]. However, the predominance of fossil fuels, especially coal, poses severe environmental and occupational risks. While coal is a dependable source of energy, its extraction is fraught with hazards, making it one of the world's most perilous occupations [2]. Coal miners are exposed to large quantities of toxic dust and are at risk of cave-ins and explosions [3]. Moreover, burning coal for energy releases a plethora of toxic byproducts and gases into the atmosphere, exacerbating ozone depletion and contributing to global warming [4].

In contrast, renewable energy sources such as solar photovoltaic (PV) panels offer a more sustainable alternative. They are safe to manufacture, emit no byproducts during operation, operate quietly, and harness the ubiquitous energy of the sun. These benefits have contributed to a 34 % increase in residential solar power installations in the United States, from 2.9 GW in 2020 to 3.9 GW in 2021 [5]. Additionally, the Kingdom of Saudi Arabia is ambitiously aiming to install 40 GW of solar PV power by 2030 through the implementation of large-scale projects exceeding 100 MW each [6]. Furthermore, Nigeria, Africa's largest economy, has seen its solar energy capacity more than double, from 15 MW in 2012 to 33 MW in 2022 [7].

Nonetheless, solar panels are not without challenges, especially in regions with high temperatures. Panel overheating significantly impairs performance due to the accelerated rate of internal carrier recombination arising from increased carrier concentrations under elevated temperatures [8]. Over the years, a variety of strategies have been proposed to enhance the cooling of solar panels for improved performance [9]. One approach that has garnered particular attention is the integration of thermoelectric generators (TEGs) with solar photovoltaic (PV) panels. TEGs not only absorb heat but also convert it into electricity, thereby harnessing the waste heat generated by solar PV panels [10,11]. This is in contrast to other cooling media, which only absorb waste heat without converting it into useable power for the hybrid system.

Numerous studies have been conducted on the performance evaluation and optimization of hybrid solar PV-TEG systems. For instance, Zhang and Gao [12] conducted an extensive review on the application of TEGs to cool solar PV panels exposed to prolonged solar irradiance. They also examined the optimization of the device's internal and external aspects for maximizing power production. Ejaz [13] explored the integration of TEGs with PV systems, focusing on optimizing the dynamic operation of the hybrid system through a generalized particle swarm optimization algorithm for maximum power generation. In another study, Lee et al. [14] employed a cooling patch to enhance the cooling rate of the PV backplate, which in turn increased the temperature gradient across the TEG in a hybrid system. They reported that under 1 Sun of irradiance, the power generation of their system increased from 19.9 mW to 24.2 mW due to the inclusion of the cooling patch. Liu et al. [15] assessed the performance of hybrid PV-TEG systems with varying glass cover coatings under different heat and light conditions, and environmental parameters such as wind speed, ambient temperature, relative humidity, and concentration ratio. They also identified potential avenues for further enhancements in system performance. Li et al. [16] aimed to mitigate efficiency losses in concentrated photovoltaic (CPV) modules by integrating TEG modules. They utilized three-dimensional numerical simulations to optimize the operating parameters of the hybrid system under laser-induced radiation and achieved an optimized efficiency of 28.9 % along with an 8 % increase in power. Liang et al. [17] developed an optimization model for a spectral-splitting CPV-TEG system, in which the TEG module maintained a two-stage cascaded structure. They constructed a theoretical model to optimize the thermoelectric geometry and optical concentration ratio for maximizing power and efficiency. At a solar irradiance of 1000 W/m^2, they achieved a combined system efficiency of 35 % with an optical concentration ratio of 1000 and a 0.6 TEG stage height ratio. Lorenzi [18] investigated the performance of a hybrid PV-TEG system under negative illumination, where the PV component cools by radiating towards the sky, and the TEG develops a temperature gradient for additional power harvesting. Lorenzi found that, similar to positive illumination, cell temperature sensitivity is the dominant operational parameter during negative illumination applications for hybrid PV-TEG systems.

Previous research on optimizing PV-TE (Photovoltaic-Thermoelectric) systems primarily focused on single-objective optimization for assessing performance. However, multi-objective optimization offers a more accurate and realistic approach, as it takes into account various target parameters such as power, efficiency, cost, and environmental impact under different operating conditions [19]. As a result, a handful of studies have ventured into multi-objective optimization of PV-TE systems to maximize performance across different target parameters under specific conditions. For example, Agba et al. [20] utilized both experiments and the Multi-Objective Genetic Algorithm (MOGA) to evaluate and optimize the performance of various PV-TE systems cooled with natural air, water, and nanofluids. Their results revealed that the nanofluid (specifically nano-silver-water) cooling medium led to a 20.68 % performance improvement in the air-cooled PV-TE system, which was the highest enhancement observed. Similarly, Ge et al. [21] employed MOGA to optimize power generation and efficiency in a PV-TE system using different cooling media. They combined numerical simulations to control the panel temperature with multi-criteria decision-making to balance output power and efficiency. The analysis demonstrated that the optimal compromise solution increased the power output by 120 % while only decreasing the system efficiency by 14 %. In another study, Yin and Li [22,23] conducted a multi-objective optimization of a spectrum-splitting CPV-TE (Concentrated Photovoltaic-Thermoelectric) system using MOGA, parameter selection, and sensitivity analysis. The critical parameters were identified through sensitivity analysis, and it was found that the maximum system efficiency was achieved with a PV bandgap of 1.42 eV.

Despite recent advancements in the field of CPV-TE systems, there is a notable lack of studies focusing on the multi-objective optimization of these systems with respect to the 4 E parameters (energy, exergy, environmental, and economic). This gap in research hinders the sustainable design and potential for mass production of CPV-TE technology. While previous studies have considered internal and external operating conditions, such as thermoelectric (TE) geometry, environmental factors, and system structure, a critical aspect that has not been sufficiently addressed is the impact of thermoelectric material properties on the overall system performance. The thermoelectric semiconductor plays a crucial role in CPV-TE systems, as it is responsible for conducting heat away from the photovoltaic (PV) backplate and generating electricity through thermoelectric effects. However, there exists a discord between the optimal material properties required for maximum performance of TEGs and PV panels. TEGs require a high Seebeck coefficient, high electrical conductivity, and low thermal conductivity for peak performance, which often necessitates sophisticated material modification techniques like doping. In contrast, effective PV cooling demands high thermal conductivity from the TEG to efficiently dissipate heat. This conflict highlights the need for a multi-objective optimization strategy that incorporates genetic and goal attainment algorithms to identify the optimal TE material for enhancing the performance of hybrid PV-TE systems. Most existing studies have primarily focused on bismuth telluride (BiTe) as the TE material, overlooking the potential of alternative materials that may outperform BiTe in hybrid PV-TE systems. This work aims to fill this knowledge gap by evaluating the impact of a diverse range of thermoelectric materials, covering high, mid, and low-temperature ranges, on the 4 E performance of a CPV-TE system under various environmental conditions and operational parameters. Moreover, this study leverages the data obtained from multi-objective optimization to train an array of regression-based machine learning models for accurate CPV-TE performance forecasting. By employing machine learning techniques, this approach facilitates rapid integration into production pipelines, accelerating the manufacturing process and enabling the mass production of these devices.

This work's novelty lies in its comprehensive evaluation of the impact of various thermoelectric materials on the 4 E performance of CPV-TE systems, the utilization of multi-objective optimization algorithms to identify optimal TE materials, and the application of machine learning models for precise performance prediction. These contributions address the existing research gaps and provide valuable insights for the sustainable design and mass production of CPV-TE technology.

2. Materials and methods

In this section, we delve into the core methodologies and materials employed in this study. Our objective is to illuminate the structured approach adopted to achieve an optimized performance of Concentrated Photovoltaic-Thermoelectric (CPV-TE) systems across different materials. The section elaborates on the selection and characteristics of the materials used for the thermoelectric elements. It also systematically discusses the mathematical modeling adopted to simulate the CPV-TE systems, as well as an in-depth explanation of the optimization algorithm deployed. Additionally, this section sheds light on the environmental and operating conditions considered, and the machine learning models developed for predictive analysis. The precision and structured nature of the methodologies described herein are foundational to the outcomes and conclusions of this research.

2.1. Mathematical modeling

The system examined in this study is a directly coupled Concentrated Photovoltaic-Thermoelectric (CPV-TE) module, in which the Thermoelectric Generator (TEG) absorbs heat energy from the back sheet of the Photovoltaic (PV) cell, as depicted in Fig. 1. Notably, this system is classified as an integrated CPV-TE system due to the elimination of the top ceramic plate that is typically present in conventional TEGs. This modification is crucial as it not only enhances heat transfer but also contributes to a more compact design compared to traditional CPV-TE systems. To further boost heat transfer, thermal grease with a thermal conductivity of 4.2 $Wm^{-1}K^{-1}$ is assumed to be interposed between the PV's back sheet (Tedlar) and the electrodes of the TEG. Consequently, the temperature at the hot side of the TEG can be considered to be approximately equal to the temperature of the back sheet. This temperature is defined as per reference [24]:where T_a (°C) represents the ambient temperature, G (W/m^2) is the solar irradiance, v (m/s) denotes the wind speed measured at a height of 10 m, and 'a' and 'b' are empirically determined coefficients. For a linear concentrator with a concentration ratio of 22, the coefficients 'a' and 'b' are found to be −3.23 and −0.13, respectively. The first term on the right-hand side of Eq. (1) is included to convert the unit of T_h from Celsius to Kelvin. The temperature of the PV can be calculated from the temperature of its back side, as described in Ref. [24]:

$T_{pv} = T_h + \frac{G\,\Delta T}{G_s}$ (2) where $G_s = 1000$ W/m^2 represents the solar irradiance measured under standard test conditions, and ΔT is the temperature difference between the surface of the PV and the back sheet at a solar irradiance of 1000 W/m^2. This temperature difference is zero

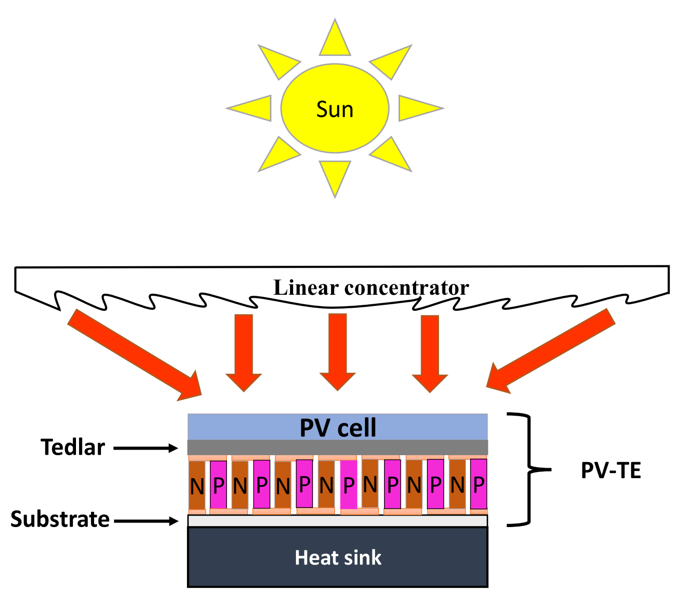

Fig. 1. An integrated CPV-TE system.

$$T_h = 273 + T_a + Ge^{a+bv} \quad (1)$$

for an insulated PV module and is 13 for a standalone PV module with a concentration ratio (C) of 22. In this study, ΔT is considered as one of the optimization variables because it depends on the thermal resistance of the TEG and the heat transfer through convection.

From **Eq. (2)**, the output power generated by the PV can be computed as:

$$P_{pv} = CGA_{pv}\tau_g\eta_r\left(1 - \beta\left(T_{pv} - 298\right)\right) \tag{3}$$

where A_{pv} (m^2) represents the surface area of the PV, τ_g is the transmissivity of the glass, η_r is the reference efficiency of the PV, and β (K^{-1}) is the temperature coefficient of the PV. The heat absorbed by the hot side and the heat released from the cold side of the TEG are given as:

$$Q_h = NI\left[S_hT_h - 0.5IR + (T_h - T_c)\left(\frac{K}{I} - 0.5\tau\right)\right] \tag{4}$$

$$Q_c = NI\left[S_cT_c + 0.5IR + (T_h - T_c)\left(\frac{K}{I} + 0.5\tau\right)\right] \tag{5}$$

The output power generated by the TEG can be determined by subtracting Eq. (5) from Eq. (4).

$$P_{TE} = NI[(S_hT_h - S_cT_c) - \tau(T_h - T_c) - IR] \tag{6}$$

where $N = 127$ represents the number of thermocouples, τ (μV/K) is the Thomson coefficient, R (Ω) denotes the internal resistance of a single thermocouple, I (mA) is the electric current flowing through a single thermocouple, T_c (K) is the temperature of the cold side, and S_h (μV/K) and S_c (μV/K) are the Seebeck coefficients of the hot and cold sides of the TEG, respectively.

The temperature of the cold side is influenced by the heat transfer through conduction from the hot side to the cold side, as well as by the heat sink on the cold side of the TEG. This can be expressed as:

$$T_c = \frac{T_h + h\,A_{te}\,R_{kt}\,(T_a + 273)}{1 + h\,A_{te}\,R_{kt}} \tag{7}$$

where h ($W/m^2 \cdot K$) represents the heat transfer coefficient, R_{kt} (K/W) denotes the thermal resistance of the TEG, and A_{te} (m^2) is the surface area of the TEG. The inclusion of the Thomson coefficient in Eqs. (4)–(6) implies that the properties of the TE materials are temperature-dependent, which is the case if the TEG operates across a significant temperature gradient. In accordance with this, the Thomson coefficient, the internal resistance of a single thermocouple, and the thermal resistance of the TEG are defined by Eqs. 8–10, respectively [25,26].

$$\tau = \frac{1}{T_h - T_c}\int_{T_c}^{T_h} S'(T)\,TdT \tag{8}$$

$$R = \frac{L(T_h - T_c)}{A}\left(\frac{1}{\int_{T_c}^{T_h}\sigma_p(T)dT} + \frac{1}{\int_{T_c}^{T_h}\sigma_n(T)dT}\right) + R_{con} \tag{9}$$

$$R_{KTE} = \frac{L(T_h - T_c)}{N\,A\left(\int_{T_c}^{T_h}\kappa_p(T)dT + \int_{T_c}^{T_h}\kappa_n(T)dT\right)} \tag{10}$$

where $S'(T)$ represents the derivative of the Seebeck coefficients with respect to temperature, T (K) is the absolute temperature, k_p and k_n are the thermal conductivities, and σ_p and σ_n are the electrical conductivities of the p-type and n-type TE legs, respectively. L represents the length of the TE leg, A (m^2) is the cross-sectional area of a TE leg, and R_{con} (Ω) is the contact resistance. The energy efficiency of the system is defined as the ratio of the output power to the input energy:

$$\eta_{sys} = \frac{P_{pv} + P_{pv}}{CGA_{pv}} \tag{11}$$

while the maximum useful work that the PV and TEG can accomplish to bring the CPV-TE system into equilibrium with its surroundings is known as the exergy of the system [27,28]. The exergy efficiency of the CPV-TE system is related to the energy efficiency of the system as follows:

$$\Psi_{sys} = \frac{\eta_{sys}}{\left[1 - \frac{4}{3}\frac{T_a}{T_s} + \frac{1}{3}\left(\frac{T_a}{T_s}\right)^4\right]} \tag{12}$$

The annual average energy produced by the CPV-TE system can be calculated by taking into account the average daily sunshine hours and the instantaneous power. In this study, an average daily sunshine duration of 10 h is assumed in Northern Nigeria. We acknowledge that the actual daily sunshine hours may vary throughout the year due to seasonal changes and weather conditions. However, for the purpose of providing a representative estimate of the annual energy generation potential, we have used the average daily sunshine hours specific to the location.

Consequently, the annual energy is given by:

$$E_{sys} = \int_0^t \left(P_{pv} + P_{te}\right)dt \tag{13}$$

Carbon dioxide (CO_2) emissions are reduced through energy generation by the CPV-TE system. The annual amount of CO_2 saved, considering fossil fuel as the alternative energy source, is calculated as follows:

$$CO_{2saving/year} = cde_{ele}E_{sys} \tag{14}$$

where cde_{ele} is the coefficient of CO_2 saving set at 0.475 kg/kWh [29].

Additionally, conducting a cost analysis is essential to evaluate the viability of an investment. Various financial metrics such as payback period (PBP), capital recovery factor (CRF), levelized cost of energy (LCOE), net present value (NPV), and internal rate of return (IRR) can be employed to assess the economic feasibility of an energy system. In this study, the undiscounted PBP, which indicates the number of years required for the CPV-TE system to recoup the initial investment, is utilized and defined as follows [30]:

$$PBP = \frac{\ln\left[1 + \frac{C_i\ i_f}{E_{sys}\ E_c}\right]}{ln\left[1 + i_f\right]} \tag{15}$$

where C_i ($) represents the initial investment, i_f denotes an inflation rate of 8 %, and E_c is the first-year energy cost, amounting to 0.149 $\$(kWh)^{-1}$ [31]:

2.2. Optimization of CPV-TE system

In optimizing energy systems, it is imperative to select the most efficient thermoelectric (TE) material for fabricating thermoelectric generators (TEGs) within CPV-TE systems to maximize energy generation, prolong system lifespan, and reduce energy costs. This study embarks on a novel simultaneous optimization of exergy efficiency (Eq. (12)) and annual energy (Eq. (13)) for CPV-TE systems employing diverse TE materials including bismuth telluride (BiTe)-based, nanomaterial-based, cobalt antimonide (CoSb)-based, lead telluride (PbTe), higher manganese silicide (HMS), and lithium nickel oxide (LiNiO). Fig. 2a), 2 b), and 2c) depict the transport properties of these TE materials. A cutting-edge hybrid multi-objective algorithm combining goal attainment and genetic algorithms (in MATLAB toolbox) is employed for optimization [32,33]. This hybrid approach capitalizes on the strengths of both algorithms, with goal attainment initially defining the search space and genetic algorithm refining the search. Eight variables are defined for optimization, with four pertaining to the PV (solar irradiance, wind speed, ambient temperature, and temperature difference between the PV surface and back sheet) and four to the TEG (electric current, length of thermoelement, area of thermoelement, and

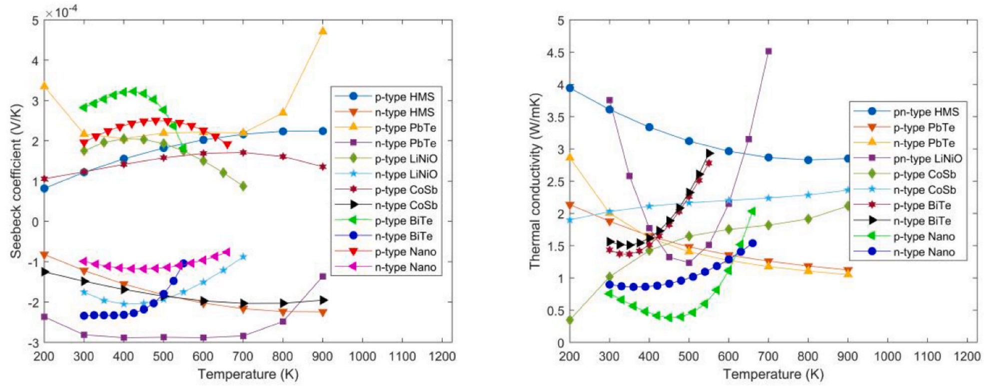

Fig. 2. Temperature dependent properties of the various thermoelectric materials [34–40].

heat transfer coefficient). The PV-related variables' range is based on Katsina city, Nigeria's annual weather data, while the TEG-related variables' range reflects typical commercial TE devices. The variables are constrained within the ranges presented in Table 1.

The properties of the thermoelectric materials are provided in Fig. 2 and Table 2 while the parameters and cost of the PV and CPV-TE systems are given in Table 3 and Table 4, respectively.

2.3. Simplifications of the CPV-TE model

In this study, several simplifying assumptions are employed in the CPV-TE model for computational tractability:

1. Steady-state heat transfer is assumed.
2. Adiabatic side boundaries are assumed for the PV.
3. The contact resistance of the TEG is considered to be 10 % of its internal resistance.
4. For the TEG, convection and radiation losses are considered negligible.

2.4. Machine learning dataset

A dataset comprising features of six different materials is generated for the development of various machine learning (ML) techniques. The dataset encompasses 1400 data points for each material and includes the following features:

1. Solar irradiance (G) in W/m^2.
2. Wind speed measured at a height of 10 m (v) in m/s.
3. Ambient temperature (T_a) in °C.
4. Electric current of a unicouple (I) in mA.
5. Length of the TE leg (L) in mm.
6. Area of PV/TEG (A_{pv}) in mm^2.
7. Thermal conductivity (h) in W/(m^{2}K).
8. Temperature difference between the surface of the PV and the back sheet at a solar irradiance of 1000 W/m^2 (ΔT) in °C.

Table 1
Parameter ranges.

Symbol	Description	Range	Units
G	Solar irradiance	$200 \le G \le 1000$	W/m^2
v	Velocity	$2 \le v \le 11$	m/s
Ta	Ambient Temperature	$288.15 \le Ta \le 313.15$	K
ΔT	Temperature Difference	$276.15 \le \Delta T \le 293.15$	K
I	Current	$0.001 \le I \le 0.1$	A
L	Length	$0.0005 \le L \le 0.004$	m
A	Area	$0.000001 \le A \le 0.000005$	m^2
h	Heat Transfer Coefficient	$100 \le h \le 2000$	W/(m^2·K)

Table 2
Temperature dependent electrical conductivities of the various thermoelectric materials [34–40].

S/N	Material	Electrical conductivity (S/m)
1.	HMS	$-7.82 \times 10^4 - 128.17T + 7.45 \times 10^{-2}T^2$
2.	*n*-type PbTe	$146{,}200 - 1041.9T + 3.13157T^2 - 404.29 \times 10^{-5}T^3 + 190.34 \times 10^{-8}T^4$
3.	*p*-type PbTe	$17{,}902 + 1233.6T - 4.2167T^2 + 512.9 \times 10^{-5}T^3 - 214.35 \times 10^{-8}T^4$
4.	LiNiO	$-1.68 \times 10^7 + 2.15 \times 10^5T - 1.08 \times 10^3T^2 + 2.69T^3 - 3.31 \times 10^{-3}T^4 + 1.62 \times 10^{-6}T^5$
5.	*n*-type CoSb	$2.9221 \times 10^{-6} + 1.5542 \times 10^{-8}T - 4.7078 \times 10^{-12}T^2 - 4.1703 \times 10^{-15}T^3$
6.	*p*-type CoSb	$6.5155 \times 10^{-6} - 2.3672 \times 10^{-9}T + 2.6624 \times 10^{-11}T^2 - 2.0732 \times 10^{-14}T^3$
7.	*n*-type BiTe	$1.60117 \times 10^{-5} - 0.01853 \times 10^{-5}T + 7.77051 \times 10^{-10}T^2 - 7.75456 \times 10^{-13}T^3$
8.	*p*-type BiTe	$7.75456 \times 10^{-5} - 1.715 \times 10^{-7}T + 6.09155 \times 10^{-10}T^2 - 6.04782 \times 10^{-13}T^3$
9.	*n*-type Nano	$-4 \text{ x } 10^{-6} + 8 \times 10^{-8}T - 2 \times 10^{-10}T^2 + 2 \times 10^{-13}T^3$
10.	*p*-type Nano	$-2 \text{ x } 10^{-7} + 7 \times 10^{-9}T + 7 \times 10^{-11}T^2$

Table 3
Parameters of the PV [41].

Parameter	Symbol	Value
Area of PV/TEG	A_{pv}	16×10^{-4} m^2
Efficiency temperature coefficient of PV	β	45×10^{-3} K^{-1}
Efficiency at standard test conditions	η_r	15.6 %
Transmissivity of glass	τ_g	0.95

Table 4
Cost of the CPV-TE system [42].

Item	Price ($)
Fresnel lens	7.615
PV cell	18.277
TEG	39.599
2-axis Sun tracking system	761.522

9. Annual energy (E_{sys}) in kWh.
10. Instantaneous exergy (Ψ_{sys}) in %.
11. CO2 saving ($CO_{2saving/year}$)in kg/yr.
12. Payback period (PBP) in years.

The first eight features serve as predictors (inputs) for the ML models, while the latter four features are the targets (outputs) for the prediction tasks for each material.

Figs. 3 and 4 provide visual representations of the evolution of input and output features, respectively, by illustrating the first 100 samples for the bismuth telluride (BiTe) material.

In the study, the dataset ($\boldsymbol{X}$) is divided into three subsets: training, validation, and testing, for the purpose of building, optimizing, and evaluating the machine learning models, respectively. Specifically, out of the initial 1000 data points, 75 % are allocated for training ($\boldsymbol{X}_{train}$) and 25 % for validation ($\boldsymbol{X}_{valid}$), using the 25 % Holdout validation procedure. The remaining 400 data points constitute the testing dataset ($\boldsymbol{X}_{test}$). Furthermore, Principal Component Analysis (PCA) [43] is utilized to enhance prediction performance by selecting features that account for 95 % of the variance in the target variables [44], thus ensuring dimensionality reduction. For cases with stronger dimensionality, alternative methods such as the kernel PCA may be more suitable.

2.5. Machine learning prediction methodology

In this study, a range of Machine Learning (ML) techniques are deployed to predict the performance of a proposed energy system. Specifically, these ML techniques are focused on independently predicting four parameters of the system: annual energy (in kWh), instantaneous exergy (in %), yearly CO_2 saving (in kg/year), and payback period (in years).

The ML techniques that have been explored include:

1. Regression Trees (RTs)
2. Ensembles of Regression Trees (ERTs)
3. Support Vector Machines (SVMs)
4. Gaussian Process Regression (GPR)
5. Neural Networks (NN)

These ML techniques have been implemented through the Regression Learner App that is available in the Machine Learning and Deep Learning toolbox of MATLAB software (version 2021b) [45]. Furthermore, these algorithms were optimized in terms of their configurations and hyperparameters through the Bayesian Optimization process across 30 iterations.

In order to evaluate the predictive capabilities of the ML models, two standard performance metrics have been employed - the Root Mean Square Error (RMSE) and the Mean Absolute Error (MAE) [46]. Both metrics were computed on validation and test datasets.

- RMSE is an indicative measure of the average magnitude of errors between the predicted and actual observations, squaring the average difference.
- MAE provides a direct average measure of the absolute errors between the predicted and actual observations.

The focus of employing these metrics is to gauge the accuracy and reliability of the ML models in predicting the proposed system's performance parameters. Once the ML algorithms are optimized and the best-performing model is identified based on the validation dataset, this model is then used to estimate the system's performance parameters using the test dataset.

3. Results and Discussions

In the forthcoming Results and Discussion section, we shall delve into an in-depth examination and analysis of the key findings emanating from the research. Initially, the section sheds light on the optimization of the Concentrated Photovoltaic and Thermoelectric (CPV-TE) systems, incorporating six varied TE materials, and scrutinizes their influence on the system's cooling and 4 E (energy, exergy, environmental, and economic) performance. The TE materials in focus, namely BiTe, PbTe, HMS, CoSb, LiNiO, and nanomaterials, have been selected to cover a range of applications including high, mid, and low-temperature scenarios.

Subsequently, the section discusses the application of multi-objective optimization algorithms, which combine genetic and goal decision algorithms, for determining the optimal combination of CPV and TEG parameters that yield the highest 4 E performance. These optimized parameters include solar irradiance, wind speed, ambient temperature, temperature difference across the PV, electric current, length and area of thermoelement, and cooling heat transfer coefficient.

Moving further, the Results and Discussion section critically evaluates the application of Machine Learning (ML) techniques for predictive modeling of the system's performance. Five regression-based ML models, namely Regression Trees (RT), Ensembles of Regression Trees (ERT), Support Vector Machines (SVM), Gaussian Process Regression (GPR), and Neural Networks (NN), have been examined. The predictive accuracy of these models is analyzed using Root Mean Square Error (RMSE) and Mean Absolute Error (MAE) metrics.

Lastly, the section engages in a comparative analysis of the performance of the different TE materials under varying conditions, highlighting the scenarios where specific materials outperform others. It also

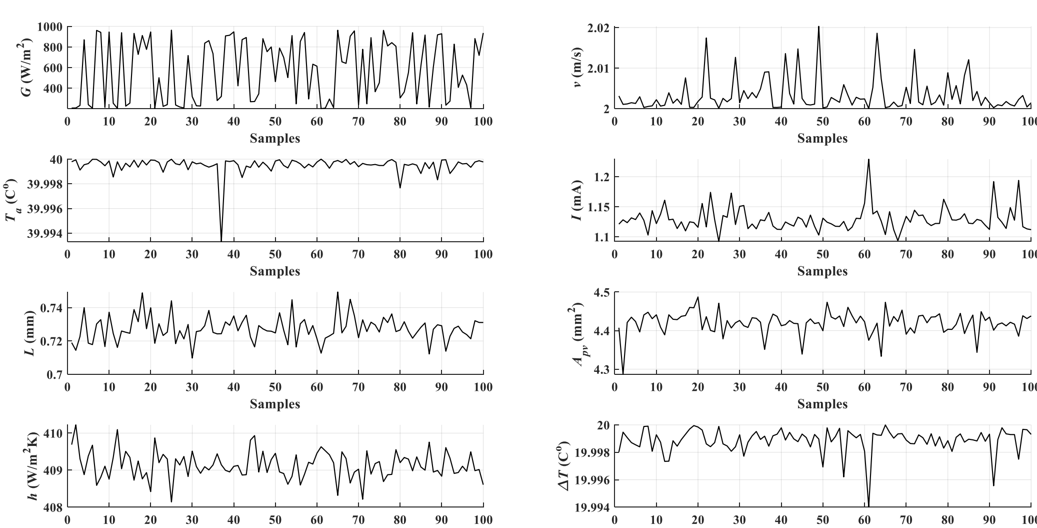

Fig. 3. Input features' evolution.

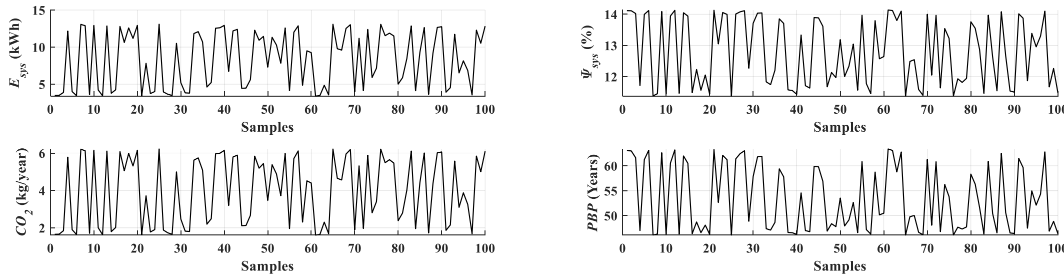

Fig. 4. Output features' evolution.

discusses the implications of these findings, particularly in terms of their practical applications and impact on the environment and economics.

Insights garnered from this section are crucial in understanding the optimal design criteria for CPV-TE systems and pave the way for advancements in their efficiency and sustainability.

3.1. Model validation

The model developed in this study is validated against experimental data from the work of Zhang et al. [47], as depicted in Fig. 5a and b. For the validation, a scenario is considered where the product of the concentration ratio and solar irradiance is 3500 W/m^2. Additionally, it is assumed that both the ambient temperature and the temperature of the cooling water are set at 25 °C.

Three different cases are taken into account for this validation, focusing on the thermal grease that is sandwiched between the Photovoltaic (PV) and the Thermoelectric Generator (TEG). These cases are characterized by varying thermal conductivities of the thermal grease: 0, 1, and 4.2 W/m·K.

The results depicted in Fig. 5a and b demonstrate that as the thermal conductivity of the thermal grease increases, the output power of the CPV-TE system also rises. This increase in output power is attributed to the enhancement of heat transfer from the back sheet of the PV to the electrodes on the hot side of the TEG.

In conclusion, the model developed in this study exhibits a high degree of agreement with the experimental data. This indicates that the model is reliable and can be effectively used for the analysis of a CPV-TE system.

3.2. Multi-objective optimization results

Fig. 6 displays the Pareto optimal front of the optimized CPV-TE (Concentrated Photovoltaic-Thermoelectric) system with various thermoelectric (TE) materials. The Pareto front illustrates the trade-off between exergy efficiency and annual energy output of the system. The exergy efficiencies range from 11 to 14.2 %, while the annual energy

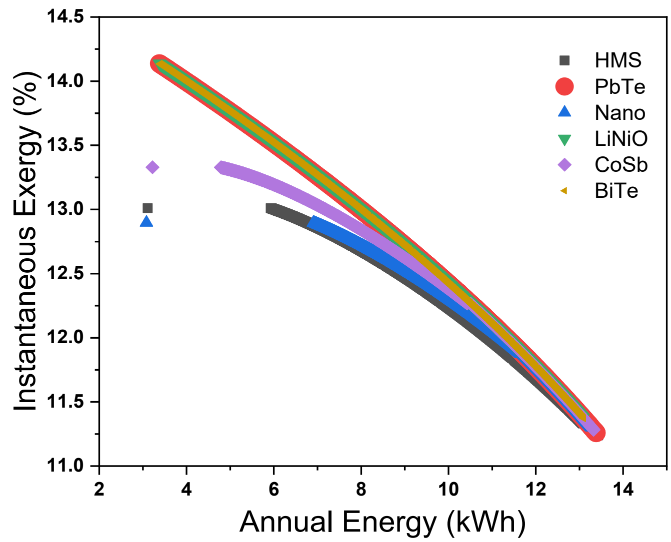

Fig. 6. Pareto optimal front.

output varies between 3 and 13.5 kWh. These variations can be attributed to the distinct properties of the TE materials used in the CPV-TE system.

From the Pareto front, it is observed that the highest exergy efficiency of 14.2 % is achieved with PbTe, LiNiO, and BiTe-based TE materials, whereas the lowest is observed with HMS TE material. Regarding annual energy, the system with PbTe as the TE material exhibits the highest annual energy output of 13.5 kWh, while the one with LiNiO records the lowest at 13 kWh. Since the points on the Pareto front represent various trade-offs between exergy efficiency and annual energy, the selection of an optimal point depends on the designer's preference between these two performance metrics. It is concluded that the model using PbTe TE material demonstrates the best performance,

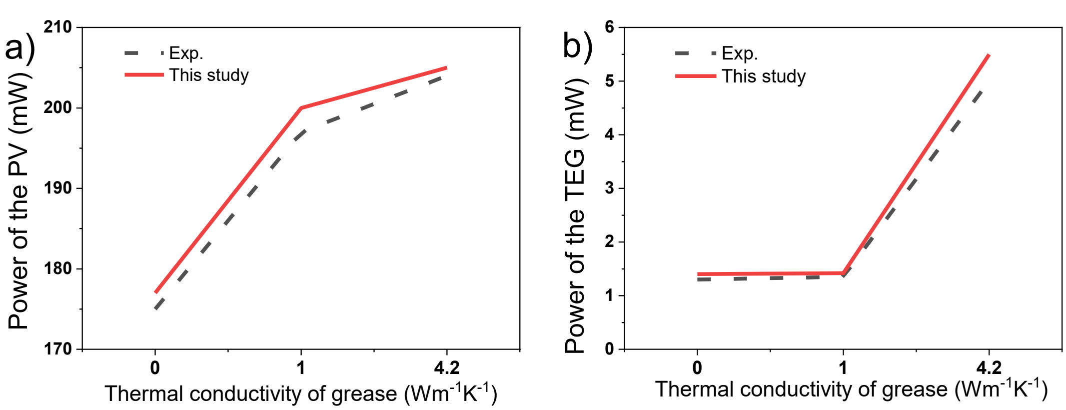

Fig. 5. Validation of the present study.

making it a suitable choice for implementation in the CPV-TE system.

Upon completion of the hybrid algorithm, the Pareto optimal front (shown in Fig. 6) is accompanied by the associated optimized variables presented in Table 5. Analyzing the data of the optimized variables, it is evident that solar irradiance exhibits significant variation across all cases. However, ambient temperature, wind speed, and temperature difference between the top and back sides of the PV stabilize around optimal values of 39.9 °C, 2 m/s, and 19.9 °C, respectively. Similarly, each CPV-TE model has optimal values for the length and area of the thermoelement, heat transfer coefficient, and electric current.

It is noted that there is an inverse relationship between the length of the thermoelement and its area for each TE material. This can be attributed to the thermal resistance and internal resistance associated with each TE material. In each scenario, the algorithm identifies the optimal geometry that offers the best balance between thermal resistance and internal resistance. Models with shorter thermoelements and/or lower electric current might need a smaller heat transfer coefficient compared to models with longer thermoelements due to the higher thermal resistance in the former. Higher thermal resistance leads to a greater temperature gradient across the TEG, and consequently, a higher temperature for the PV.

Fig. 7a to f depict the variations in annual CO_2 savings and the payback period (PBP) of the CPV-TE (Concentrated Photovoltaic-Thermoelectric) system. These two metrics are calculated based on the optimized annual energy output of the CPV-TE system. The annual CO_2 savings range from 1.5 to 6.4 kg/year, while the payback periods are observed to be between 45 and 65 years.

For an energy system to be considered ideal, it should have high CO_2 saving potentials along with a low payback period. Among the different models, the ones using PbTe and HMS as thermoelectric materials yield the highest CO_2 savings, achieving 6.4 kg/year. Since the cost of the thermoelectric generator (TEG) is assumed to be constant regardless of the thermoelectric material used, the payback periods are found to be nearly identical across all models.

However, it is critical to note that the CPV-TE models typically have an operational lifespan of around 20 years. Given that the payback periods exceed this lifespan, none of the models appear to be economically feasible despite the optimization efforts. This assessment could change if the initial cost of the CPV-TE system is reduced by at least 60 % and if there are advancements in the performance of thermoelectric materials. The lengthy payback period is one of the factors contributing to the reluctance of investors to engage in integrated CPV-TE systems, as compared to the more traditional flat-plate PV modules.

3.3. Machine learning prediction results

Table 6 presents the optimal machine learning (ML) techniques selected for predicting each performance parameter of the six thermoelectric materials investigated in this study. The selection was based on the validation dataset, which was used to assess the performance of various ML models, including Regression Trees, Ensembles of Regression Trees, Support Vector Machines, Gaussian Process Regression (GPR), and Neural Networks (NN). The table also includes the optimal technical characteristics identified for each technique, along with the performance metrics computed using the validation dataset.

Among the ML techniques explored, GPR consistently demonstrated the highest accuracy in estimating the system's performance parameters across all six materials. This finding is supported by our previous work [48], which extensively discusses the computation and evaluation of different metrics, such as Root Mean Square Error (RMSE) and Mean Absolute Error (MAE), to compare the performance of various ML models. The superior performance of the GPR model can be attributed to its ability to capture complex, non-linear relationships between input features and output parameters, as well as its capability to provide uncertainty estimates for its predictions.

However, it is important to note that GPR is computationally more demanding compared to other ML techniques, particularly Neural Networks (NN). The computational complexity of GPR scales cubically with the number of training samples, which can limit its applicability in scenarios with large datasets or real-time prediction requirements. In contrast, NN models, once trained, can provide faster predictions and may be more suitable for resource-constrained environments or applications requiring low-latency responses.

After the optimal models were determined, they were evaluated using the test dataset for each material. Table 7 presents the performance metrics obtained by the optimal ML techniques for each performance parameter of each material. The data in Table 7 underscores the effectiveness of the optimally tuned GPR in accurately estimating the performance parameters across the different materials.

For illustration, Fig. 8 displays the estimated values of the four performance parameters for the BiTe material. Upon examination of Fig. 8, one can observe a close match between the actual or true values of the performance parameters and the estimates produced by the optimal ML technique. These models can be employed to estimate the performance parameters of the system for any new, previously unseen data points. As a demonstration, the optimized GPR model for the BiTe material, which was developed using the training and validation datasets. This model serves as an example and can be used for validation purposes.

Table 5
Optimized parameters of the CPV-TE systems.

Parameter	BiTe	HMS	Nano	CoSb	LiNiO	PbTe
G (W/m^2)	Varies	Varies	Varies	Varies	Varies	Varies
T_a (°C)	39.9	39.9	39.9	39.9	39.9	39.9
v (m/s)	2	2	2	2	2	2
ΔT (°C)	19.9	19.9	19.9	19.9	19.9	19.9
L (mm)	0.72	3.9	3.9	3.8	0.7	0.56
A (mm^2)	4.4	1	1	1	4.4	4.8
h (W/(m^{2}K))	409	549	697	565	336	626
I (mA)	1.12	99.9	99.9	95	1.65	1.15

4. Conclusions

This study embarked on a rigorous exploration of Concentrated Photovoltaic and Thermoelectric (CPV-TE) systems, scrutinizing their performance under the influence of different thermoelectric materials. The assessment was grounded in a multi-objective optimization framework, encapsulating energy, exergy, environmental, and economic (4 E) dimensions. Based on the results of the study, the following conclusions are made:

- *Exhaustive Assessment of TE Materials*: By investigating six distinct thermoelectric materials—BiTe, PbTe, HMS, CoSb, LiNiO, and nanomaterials—across a wide temperature range, the study provides valuable insights into their individual and comparative performance. Notably, the study identified PbTe as the most promising material, delivering the highest annual energy (13.5 kWh) and featuring prominently in the top performers for exergy efficiency (14.2 %).
- *Multi-objective Optimization*: Utilizing a genetic algorithm coupled with a goal decision algorithm, the study meticulously optimized crucial CPV and TEG parameters. The optimized variables delivered an array of system configurations, unveiling an optimal balance between system efficiency and performance.
- *Eco-Friendly and Economic Considerations*: The research extended beyond energy and exergy efficiency, recognizing the importance of environmental conservation and economic viability. PbTe and HMS TE materials marked their footprint in these regards, recording the highest carbon-saving potential (6.4 kg/yr). However, the study highlighted the need for reducing the system cost by at least 60 % to make it economically feasible, given the long payback period observed.

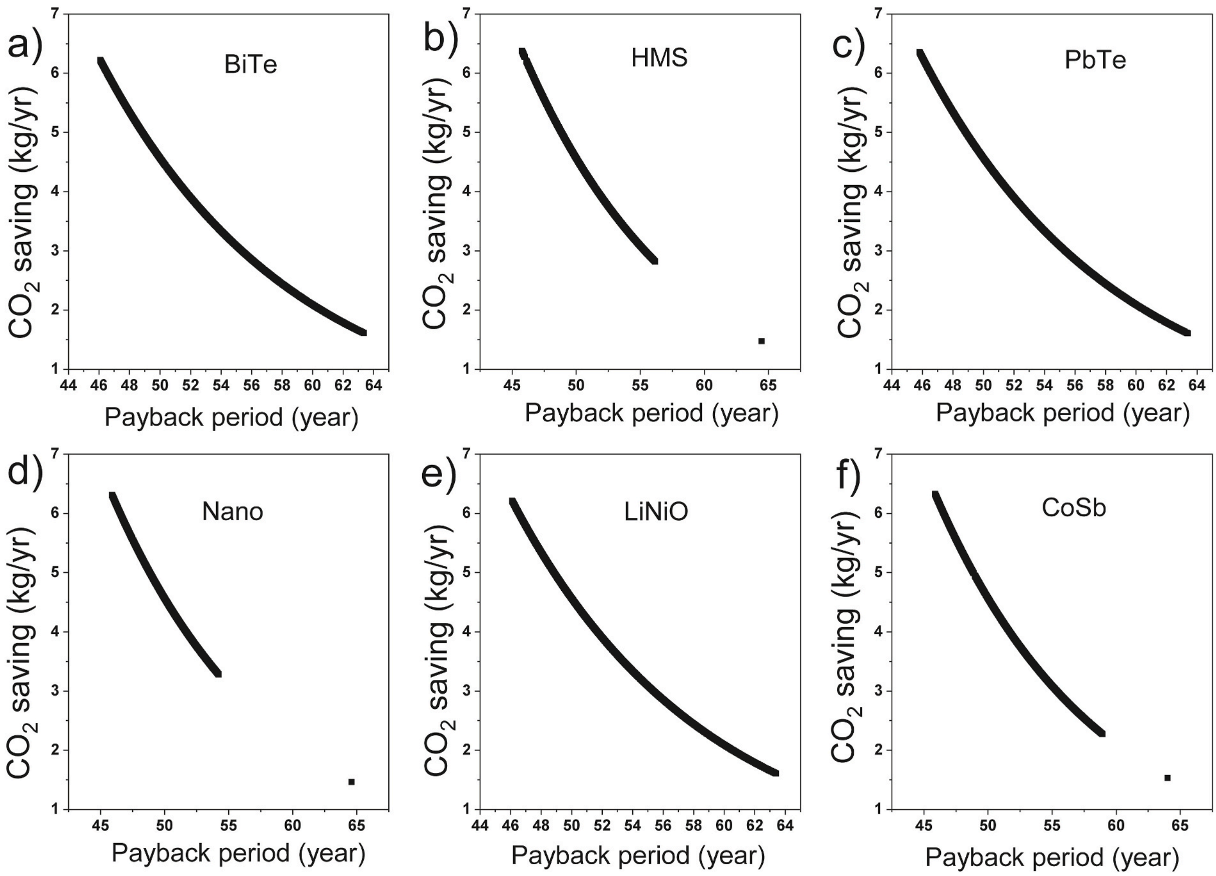

Fig. 7. CO_2 saving against payback period of the CPV-TE with a) BiTe, b) HMS, c) PbTe, d), Nano, e) LiNiO, f) CoSb material.

- *Machine Learning Proficiency*: Finally, the deployment of machine learning models demonstrated the power of advanced computational approaches in predicting system performance. The Gaussian Process Regression (GPR) model emerged as the most accurate, albeit with substantial computational requirements, hence underlining the trade-off between precision and computational expense.

In conclusion, this comprehensive exploration of CPV-TE systems provides novel insights into the role of thermoelectric materials, the importance of multi-objective optimization, the balance between ecological and economic considerations, and the potent capacity of machine learning models in performance prediction. These findings lay a robust foundation for future work, moving us closer to the goal of optimized, eco-friendly, and economically feasible CPV-TE systems.

5. Future research directions

In the present study, we have delved into the performance optimization of a concentrated photovoltaic-thermoelectric (CPV-TE) system by employing genetic algorithms, goal attainment methods, and machine learning models. The investigation focused on evaluating the CPV-TE system across multiple performance criteria, including energy, exergy, environmental, and economic aspects. As this domain is rich with opportunities for exploration and innovation, it is essential to contemplate the avenues that future research can embark upon to augment the development and feasibility of CPV-TE systems. Herein, we highlight several promising research directions that could not only address the limitations of the current study but also contribute to the advancement of CPV-TE systems in terms of performance, viability, and adaptability to different applications and environments.

- *Incorporate Dynamic Simulations*: Future studies could incorporate dynamic simulations that consider the time-varying nature of environmental factors such as solar irradiance and ambient temperature, and assess how these fluctuations impact the performance of the CPV-TE system.
- *Explore Alternative Optimization Algorithms*: While genetic algorithms were employed in this study, there are other optimization techniques such as simulated annealing, particle swarm optimization, and differential evolution that could be explored in future work for possibly improved performance.
- *Investigate Different TE Materials*: This work considered six thermoelectric materials, but there are numerous other materials with potentially better properties. Future research could investigate new or less conventional materials and their impact on CPV-TE system performance.
- *Integration with Energy Storage*: Future studies might explore the integration of the CPV-TE system with energy storage solutions like batteries or thermal storage, and evaluate the performance and viability of such hybrid systems for more reliable energy supply.
- *Developing Custom ML Models*: This work employed standard machine learning models. However, there is room for development and testing of custom-designed machine learning models that may be specifically tailored for predicting the performance of CPV-TE systems.
- *Economic Analysis and Market Potential*: Future work could focus on conducting a thorough economic analysis, considering different market scenarios and incentive programs, to assess the financial viability and market potential of CPV-TE systems.

Table 6
The optimal ML technique selected for each performance parameter of each material.

Material	Performance Parameter	Optimal ML technique	Detailed technical characteristic	Performance metrics
BiTe	E_{sys} (kWh)	Optimizable GPR	**Basis function:** Constant **Kernel function:** Nonisotropic Matern 5/2 **Kernel scale:** 680.52 **Sigma:** 0.00061 **Standardize:** No **Number of PCs:** 1	$RMSE =$ 0.0004 $MAE =$ 0.0003
	Ψ_{sys} (%)	Optimizable GPR	**Basis function:** Linear **Kernel function:** Nonisotropic Squared Exponential **Kernel scale:** 146.04 **Sigma:** 0.13 **Standardize:** No **Number of PCs:** 1	$RMSE =$ 0.0005 $MAE =$ 0.0003
	$CO_{2saving/year}$ (kg/yr)	Optimizable GPR	**Basis function:** Constant **Kernel function:** Isotropic Matern 5/2 **Kernel scale:** 29.84 **Sigma:** 0.003 **Standardize:** No **Number of PCs:** 1	$RMSE =$ 0.0002 $MAE =$ 0.0001
	PBP (years)	Optimizable GPR	**Basis function:** Constant **Kernel function:** Isotropic Exponential **Kernel scale:** 31.32 **Sigma:** 0.02 **Standardize:** Yes **Number of PCs:** 1	$RMSE =$ 0.0008 $MAE =$ 0.0004
CoSb	E_{sys} (kWh)	Optimizable GPR	**Basis function:** Zero **Kernel function:** Nonisotropic Exponential **Kernel scale:** 42.02 **Sigma:** 0.12 **Standardize:** No **Number of PCs:** 1	$RMSE =$ 0.0011 $MAE =$ 0.0004
	Ψ_{sys} (%)	Optimizable GPR	**Basis function:** Zero **Kernel function:** Nonisotropic Exponential **Kernel scale:** 342.3 **Sigma:** 0.002 **Standardize:** Yes **Number of PCs:** 1	$RMSE =$ 0.0004 $MAE =$ 0.0003
	$CO_{2saving/year}$ (kg/yr)	Optimizable GPR	**Basis function:** Zero **Kernel function:** Nonisotropic Matern 3/2 **Kernel scale:** 0.85 **Sigma:** 0.003 **Standardize:** No **Number of PCs:** 1	$RMSE =$ 0.002 $MAE =$ 0.0006

Table 6 (*continued*)

Material	Performance Parameter	Optimal ML technique	Detailed technical characteristic	Performance metrics
	PBP (years)	Optimizable GPR	**Basis function:** Constant **Kernel function:** Nonisotropic Exponential **Kernel scale:** 647.1 **Sigma:** 0.0001 **Standardize:** Yes **Number of PCs:** 1	$RMSE =$ 0.0009 $MAE =$ 0.0004
HMS	E_{sys} (kWh)	Optimizable GPR	**Basis function:** Zero **Kernel function:** Isotropic Exponential **Kernel scale:** 16.3 **Sigma:** 0.005 **Standardize:** Yes **Number of PCs:** 1	$RMSE =$ 0.0004 $MAE =$ 0.0003
	Ψ_{sys} (%)	Optimizable GPR	**Basis function:** Constant **Kernel function:** Isotropic Exponential **Kernel scale:** 5.9 **Sigma:** 0.3 **Standardize:** Yes **Number of PCs:** 1	$RMSE =$ 0.0005 $MAE =$ 0.000
	$CO_{2saving/year}$ (kg/yr)	Optimizable GPR	**Basis function:** Zero **Kernel function:** Isotropic Matern 5/2 **Kernel scale:** 1.0 **Sigma:** 0.7 **Standardize:** Yes **Number of PCs:** 1	$RMSE =$ 0.001 $MAE =$ 0.0003
	PBP (years)	Optimizable GPR	**Basis function:** Zero **Kernel function:** Nonisotropic Squared Exponential **Kernel scale:** 0.9 **Sigma:** 2.6 **Standardize:** Yes **Number of PCs:** 1	$RMSE =$ 0.05 $MAE =$ 0.004
LiNiO	E_{sys} (kWh)	Optimizable GPR	**Basis function:** Linear **Kernel function:** Isotropic Matern 3/2 **Kernel scale:** 1.9 **Sigma:** 1.3 **Standardize:** Yes **Number of PCs:** 1	$RMSE =$ 0.0008 $MAE =$ 0.0005
	Ψ_{sys} (%)	Optimizable GPR	**Basis function:** Linear **Kernel function:** Nonisotropic Squared Exponential **Kernel scale:** 573.1 **Sigma:** 0.09 **Standardize:** Yes **Number of PCs:** 1	$RMSE =$ 0.0004 $MAE =$ 0.0003
	$CO_{2saving/year}$ (kg/yr)	Optimizable GPR	**Basis function:** Linear **Kernel function:** Nonisotropic Matern 3/2	$RMSE =$ 0.0004 $MAE =$ 0.0003

(*continued on next page*)

Table 6 (*continued*)

Material	Performance Parameter	Optimal ML technique	Detailed technical characteristic	Performance metrics
			Kernel scale: 1.06 **Sigma:** 3.5 **Standardize:** Yes **Number of PCs:** 1	
	PBP (years)	Optimizable GPR	**Basis function:** Constant **Kernel function:** Isotropic Exponential **Kernel scale:** 5.7 **Sigma:** 0.002 **Standardize:** Yes **Number of PCs:** 1	*RMSE* = 0.001 *MAE* = 0.0007
Nano	E_{sys} (kWh)	Optimizable GPR	**Basis function:** Linear **Kernel function:** Nonisotropic Exponential **Kernel scale:** 762.2 **Sigma:** 0.0001 **Standardize:** Yes **Number of PCs:** 1	*RMSE* = 0.006 *MAE* = 0.004
	Ψ_{sys} (%)	Optimizable GPR	**Basis function:** Linear **Kernel function:** Nonisotropic Matern 3/2 **Kernel scale:** 239.8 **Sigma:** 0.016 **Standardize:** Yes **Number of PCs:** 1	*RMSE* = 0.001 *MAE* = 0.001
	$CO_{2saving/year}$ (kg/yr)	Optimizable GPR	**Basis function:** Linear **Kernel function:** Nonisotropic Matern 5/2 **Kernel scale:** 17.2 **Sigma:** 0.8 **Standardize:** Yes **Number of PCs:** 1	*RMSE* = 0.003 *MAE* = 0.002
	PBP (years)	Optimizable GPR	**Basis function:** Constant **Kernel function:** Isotropic Exponential **Kernel scale:** 45.6 **Sigma:** 0.02 **Standardize:** No **Number of PCs:** 1	*RMSE* = 0.009 *MAE* = 0.006
PbTe	E_{sys} (kWh)	Optimizable GPR	**Basis function:** Constant **Kernel function:** Nonisotropic Matern 3/2 **Kernel scale:** 27.3 **Sigma:** 0.12 **Standardize:** Yes **Number of PCs:** 1	*RMSE* = 0.0006 *MAE* = 0.00033
	Ψ_{sys} (%)	Optimizable GPR	**Basis function:** Linear **Kernel function:** Isotropic Squared Exponential **Kernel scale:** 167 **Sigma:** 0.18 **Standardize:** Yes **Number of PCs:** 1	*RMSE* = 0.0004 *MAE* = 0.0003
	$CO_{2saving/year}$ (kg/yr)	Optimizable GPR	**Basis function:** Constant **Kernel function:** Nonisotropic Matern 5/2 **Kernel scale:** 35.8 **Sigma:** 0.04 **Standardize:** Yes **Number of PCs:** 1	*RMSE* = 0.0002 *MAE* = 0.0001
	PBP (years)	Optimizable GPR	**Basis function:** Zero **Kernel function:** Isotropic Exponential **Kernel scale:** 342.1 **Sigma:** 0.0001 **Standardize:** Yes **Number of PCs:** 1	*RMSE* = 0.001 *MAE* = 0.0005

Table 7
The performance metrics obtained by the optimal ML techniques of each performance parameter of each material.

Material	Performance Parameter	*RMSE*	*MAE*
BiTe	E_{sys} (kWh)	3.3e-04	2.6e-04
	Ψ_{sys} (%)	4e-04	3e-04
	$CO_{2saving/year}$ (kg/yr)	1.6e-04	1.2e-04
	PBP (years)	5.2e-04	3.2e-04
CoSb	E_{sys} (kWh)	0.001	2.2e-04
	Ψ_{sys} (%)	2.8e-04	2.1e-04
	$CO_{2saving/year}$ (kg/yr)	0.0012	3e-04
	PBP (years)	0.003	3.3e-04
HMS	E_{sys} (kWh)	0.001	2.2e-04
	Ψ_{sys} (%)	2.9e-04	2.2e-04
	$CO_{2saving/year}$ (kg/yr)	3.5e-04	1.9e-04
	PBP (years)	0.001	8.7e-04
LiNiO	E_{sys} (kWh)	6.6e-04	4.4e-04
	Ψ_{sys} (%)	4.2e-04	3e-04
	$CO_{2saving/year}$ (kg/yr)	3e-04	2.1e-04
	PBP (years)	0.001	6.4e-04
Nano	E_{sys} (kWh)	0.005	0.003
	Ψ_{sys} (%)	0.001	8.8e-04
	$CO_{2saving/year}$ (kg/yr)	0.002	0.0016
	PBP (years)	0.006	0.0036
PbTe	E_{sys} (kWh)	5e-04	3e-04
	Ψ_{sys} (%)	5e-04	3e-04
	$CO_{2saving/year}$ (kg/yr)	1.8e-04	1.3e-04
	PBP (years)	0.002	4.2e-04

Availability of data and materials

The data and codes used in this work are available upon reasonable request from the corresponding authors.

CRediT authorship contribution statement

Hisham Alghamdi: Conceptualization, Methodology, Supervision. **Chika Maduabuchi:** Writing – review & editing, Writing – original draft, Methodology. **Aminu Yusuf:** Data curation, Formal analysis, Writing – review & editing. **Sameer Al-Dahidi:** Investigation, Validation, Methodology, Writing – review & editing. **Sedat Ballikaya:** Software, Visualization. **Abdullah Albaker:** Resources, Funding acquisition. **Ahmed Alsafran:** Project administration, Supervision. **Mohammed Alghassab:** Writing – review & editing. **Emad Makki:**

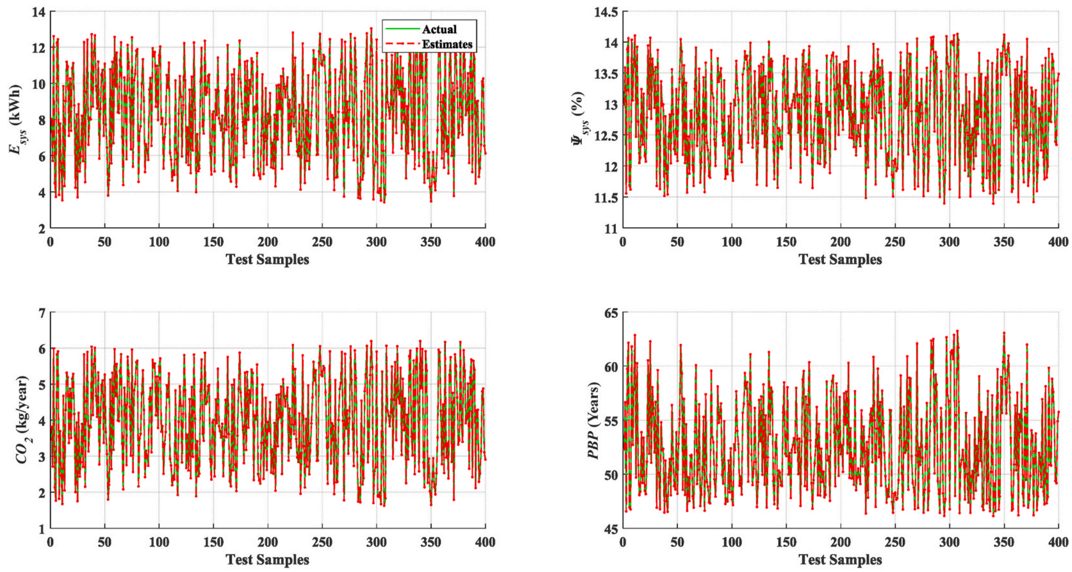

Fig. 8. Examples of the performance parameters' predictions obtained by the best optimal ML model on the test dataset of the BiTe material.

Methodology, Data curation. **Mohammad Alkhedher:** Investigation, Resources.

Declaration of competing interest

The authors declare that they have no known competing financial interests or personal relationships that could have appeared to influence the work reported in this paper.

Data availability

Data will be made available on request.

Acknowledgements

The Deanship of Scientific Research at Najran University for funding this work under the Research Groups Funding program grant code (NU/RG/SERC/12/16),the Deanship of Scientific Research at King Faisal University for funding this work under the Research Collaboration Funding program Grant Number KFU241401, the Office of Research and Sponsored Programs (ORSP) at Abu Dhabi University for funding this paper through a research fund.

References

[1] Morse E. Non-Renewable Energy | National Geographic Society n.d. https://education.nationalgeographic.org/resource/non-renewable-energy (accessed January 21, 2023).

[2] T. Liu, S. Liu, The impacts of coal dust on miners' health: a review, Environ. Res. 190 (2020) 109849, https://doi.org/10.1016/j.envres.2020.109849.

[3] R. Tong, M. Cheng, X. Yang, Y. Yang, M. Shi, Exposure levels and health damage assessment of dust in a coal mine of Shanxi Province, China, Process Saf. Environ. Protect. 128 (2019) 184–192, https://doi.org/10.1016/j.psep.2019.05.022.

[4] D. Shindell, G. Faluvegi, The net climate impact of coal-fired power plant emissions, Atmos. Chem. Phys. 10 (2010) 3247–3260, https://doi.org/10.5194/acp-10-3247-2010.

[5] Leppert R, Kennedy B. Home Solar Panel Adoption Continues to Rise in the U.S. | Pew Research Center n.d. https://www.pewresearch.org/fact-tank/2022/10/14/home-solar-panel-adoption-continues-to-rise-in-the-u-s/(accessed January 21, 2023).

[6] N. Alghamdi, A.B.S. Bahaj, P. James, Supply chain readiness for solar PV expansion in Saudi Arabia, Energies 15 (2022), https://doi.org/10.3390/en15207479.

[7] Statista Research Department. Nigeria: Solar Energy Capacity 2012-2021 | Statista n.d. https://www.statista.com/statistics/1278096/solar-energy-capacity-in-nigeria/(accessed January 21, 2023).

[8] S. Dubey, J.N. Sarvaiya, B. Seshadri, Temperature dependent photovoltaic (PV) efficiency and its effect on PV production in the world – a review, Energy Proc. 33 (2013) 311–321, https://doi.org/10.1016/j.egypro.2013.05.072.

[9] A. Machniewicz, D. Knera, D. Heim, Effect of transition temperature on efficiency of PV/PCM panels, Energy Proc. 78 (2015) 1684–1689, https://doi.org/10.1016/j.egypro.2015.11.257.

[10] P. Dwivedi, K. Sudhakar, A. Soni, E. Solomin, I. Kirpichnikova, Advanced cooling techniques of P.V. modules: a state of art, Case Stud. Therm. Eng. 21 (2020) 100674, https://doi.org/10.1016/j.csite.2020.100674.

[11] M. Sharaf, M.S. Yousef, A.S. Huzayyin, Review of cooling techniques used to enhance the efficiency of photovoltaic power systems, Environ. Sci. Pollut. Res. 29 (2022 2918 2022) 26131–26159, https://doi.org/10.1007/S11356-022-18719-9.

[12] Y. Zhang, P. Gao, Hybrid photovoltaic/thermoelectric systems for round-the-clock energy harvesting, Molecules 27 (2022) 7590, https://doi.org/10.3390/molecules27217590.

[13] M. Ejaz, Optimal control of hybrid photovoltaic-thermometric generator system using GEPSO, J. Power Energy Eng. 10 (2022) 1–21, https://doi.org/10.4236/jpee.2022.103001.

[14] J. Lee, K. Cho, Y. Park, S. Park, H.E. Song, S. Kim, Performance enhancement of hybrid energy devices using cooling patches, Int. J. Photoenergy 2022 (2022), https://doi.org/10.1155/2022/3604240.

[15] J. Liu, H. Tang, D. Zhang, S. Jiao, Z. Zhou, Z. Zhang, et al., Performance evaluation of the hybrid photovoltaic-thermoelectric system with light and heat management, Energy 211 (2020) 118618, https://doi.org/10.1016/j.energy.2020.118618.

[16] Y. Li, Z. Zhang, H. Zhang, Z. Xiao, L. Luming, P. Jiang, Numerical and experimental performance evaluation of a laser-concentrated photovoltaic-thermoelectric generator hybrid system, Opt Express 30 (2022) 19465, https://doi.org/10.1364/OE.456559.

[17] D. Liang, Q. Luo, P. Li, Y. Fu, L. Cai, P. Zhai, Optimization and experimentation of concentrating photovoltaic/cascaded thermoelectric generators hybrid system using spectral beam splitting technology, IOP Conf. Ser. Earth Environ. Sci. 199 (2018) 052044, https://doi.org/10.1088/1755-1315/199/5/052044.

[18] B. Lorenzi, Hybrid thermoelectric-photovoltaic generators under negative illumination conditions, ACS Appl. Energy Mater. (2021), https://doi.org/10.1021/acsaem.1c02710.

[19] M. Shoaei, S.F. Moosavian, A. Hajinezhad, 4E analysis of a concentrating photovoltaic thermal system (CPVT) with examining the effects of flow regime and concentration ratio, Energy Rep. 8 (2022) 14753–14770, https://doi.org/10.1016/j.egyr.2022.11.026.

[20] A. Akbar, G. Najafi, S. Gorjian, A. Kasaeian, M. Mazlan, Performance enhancement of a hybrid photovoltaic-thermal-thermoelectric (PVT-TE) module using nanofluid-based cooling: indoor experimental tests and multi-objective optimization, Sustain. Energy Technol. Assessments 46 (2021) 101276, https://doi.org/10.1016/j.seta.2021.101276.

[21] Y. Ge, Q. Xiao, W. Wang, Y. Lin, S.M. Huang, Design of high-performance photovoltaic-thermoelectric hybrid systems using multi-objective genetic algorithm, Renew. Energy 200 (2022) 136–145, https://doi.org/10.1016/j.renene.2022.09.091.

[22] E. Yin, Q. Li, Multi-objective optimization of a concentrated spectrum splitting photovoltaic-thermoelectric hybrid system, Appl. Therm. Eng. 219 (2023) 119518, https://doi.org/10.1016/j.applthermaleng.2022.119518.

[23] E. Yin, Q. Li, Device performance matching and optimization of photovoltaic-thermoelectric hybrid system, Energy Convers. Manag. X 12 (2021) 100115, https://doi.org/10.1016/j.ecmx.2021.100115.

[24] D.L. King, W.E. Boyson, J.A. Kratochvil, Photovoltaic array performance model, SANDIA Report SAND2004-3535, Sandia Rep No 2004-3535 8 (2004) 1–19.

[25] A. Yusuf, S. Ballikaya, Electrical, thermomechanical and cost analyses of a low-cost thermoelectric generator, Energy 241 (2022) 122934, https://doi.org/10.1016/j.energy.2021.122934.

[26] A. Yusuf, S. Ballikaya, Thermal resistance analysis of trapezoidal concentrated photovoltaic – thermoelectric systems, Energy Convers. Manag. 250 (2021) 114908, https://doi.org/10.1016/j.enconman.2021.114908.
[27] A. Duran Sahin, I. Dincer, M.A. Rosen, Thermodynamic analysis of solar photovoltaic cell systems, Sol. Energy Mater. Sol. Cells 91 (2007) 153–159, https://doi.org/10.1016/j.solmat.2006.07.015.
[28] A. Yusuf, S. Ballikaya, Exergy analysis of a novel concentrated photovoltaic-thermoelectric system, Int. J. Exergy 39 (2022) 117, https://doi.org/10.1504/IJEX.2022.124748.
[29] Global Energy & CO2 Status Report 2019 – Analysis 2022. https://www.iea.org/reports/global-energy-co2-status-report-2019/emissions.
[30] W.A. Beckman, N. Blair, J.A. Duffie, Solar engineering of thermal processes, photovoltaics and wind. Sol Eng Therm Process Photovoltaics Wind Fifth, fifth ed., 2021, pp. 1–905, https://doi.org/10.1002/9781119540328.
[31] Short-Term Energy Outlook - U.S. Energy Information Administration (EIA) n.d. https://www.eia.gov/outlooks/steo/report/electricity.php (accessed January 17, 2023).
[32] Effects of Multiobjective Genetic Algorithm Options - MATLAB & Simulink n.d. https://www.mathworks.com/help/gads/gamultiobj-options-effects.html (accessed January 17, 2023).
[33] When to Use a Hybrid Function - MATLAB & Simulink n.d. https://www.mathworks.com/help/gads/when-to-use-hybrid-function.html (accessed January 17, 2023).
[34] Y. Thimont, S. LeBlanc, The impact of thermoelectric leg geometries on thermal resistance and power output, J. Appl. Phys. 126 (2019) 095101, https://doi.org/10.1063/1.5115044.
[35] H. Ali, B. Sami, F.A. Al-sulaiman, Segmented thermoelectric generator : In fl uence of pin shape con fi guration on the device performance, Energy 111 (2016) 439–452, https://doi.org/10.1016/j.energy.2016.06.003.
[36] G. Zhang, L. Fan, Z. Niu, K. Jiao, H. Diao, Q. Du, et al., A comprehensive design method for segmented thermoelectric generator, Energy Convers. Manag. 106 (2015) 510–519, https://doi.org/10.1016/j.enconman.2015.09.068.
[37] W. Chen, Y. Chiou, Geometry design for maximizing output power of segmented skutterudite thermoelectric generator by evolutionary computation, Appl. Energy 274 (2020) 115296, https://doi.org/10.1016/j.apenergy.2020.115296.
[38] L.-D. Zhao, B.-P. Zhang, J.-F. Li, M. Zhou, W.-S. Liu, J. Liu, Thermoelectric and mechanical properties of nano-SiC-dispersed Bi2Te3 fabricated by mechanical alloying and spark plasma sintering, J. Alloys Compd. 455 (2008) 259–264, https://doi.org/10.1016/j.jallcom.2007.01.015.
[39] B. Poudel, Q. Hao, Y. Ma, Y. Lan, A. Minnich, B. Yu, et al., High-thermoelectric performance of nanostructured bismuth antimony telluride bulk alloys, Science 320 (80) (2008) 634–638, https://doi.org/10.1126/science.1156446.
[40] O. Högblom, R. Andersson, Analysis of thermoelectric generator performance by use of simulations and experiments, J. Electron. Mater. 43 (2014) 2247–2254, https://doi.org/10.1007/s11664-014-3020-x.
[41] P. Motiei, M. Yaghoubi, E. GoshtashbiRad, A. Vadiee, Two-dimensional unsteady state performance analysis of a hybrid photovoltaic-thermoelectric generator, Renew. Energy 119 (2018) 551–565, https://doi.org/10.1016/j.renene.2017.11.092.
[42] E. Yin, Q. Li, Y. Xuan, Feasibility analysis of a concentrating photovoltaic-thermoelectric-thermal cogeneration, Appl. Energy 236 (2019) 560–573, https://doi.org/10.1016/j.apenergy.2018.12.019.
[43] S. Wold, K. Esbensen, P. Geladi, Principal component analysis, Chemometr. Intell. Lab. Syst. 2 (1987) 37–52, https://doi.org/10.1016/0169-7439(87)80084-9.
[44] Regression Learner App - MATLAB & Simulink n.d. https://www.mathworks.com/help/stats/regression-learner-app.html (accessed July 10, 2022).
[45] Regression Learner App - MATLAB & Simulink n.d. https://www.mathworks.com/help/stats/regression-learner-app.html (accessed January 17, 2023).
[46] Z. Hajabdollahi Ouderji, R. Gupta, A. Mckeown, Z. Yu, C. Smith, W. Sloan, et al., Integration of anaerobic digestion with heat Pump: machine learning-based technical and environmental assessment, Bioresour. Technol. 369 (2023) 128485, https://doi.org/10.1016/j.biortech.2022.128485.
[47] J. Zhang, H. Zhai, Z. Wu, Y. Wang, H. Xie, Experimental investigation of novel integrated photovoltaic-thermoelectric hybrid devices with enhanced performance, Sol. Energy Mater. Sol. Cells 215 (2020) 110666, https://doi.org/10.1016/j.solmat.2020.110666.
[48] H. Alghamdi, C. Maduabuchi, A. Yusuf, S. Al-Dahidi, A. Albaker, I. Alatawi, T. R. Alsenani, A.S. Alsafran, M. AlAqil, M. Alkhedher, Multiobjective optimization and machine learning algorithms for forecasting the 3E performance of a concentrated photovoltaic-thermoelectric system, Int. J. Energy Res. 2023 (2023) e6418897, https://doi.org/10.1155/2023/6418897.